A quantitative screen for metabolic enzyme structures reveals patterns of assembly across the yeast metabolic network

Chalongrat Noree[a,b], Kyle Begovich[a,c], Dane Samilo[c], Risa Broyer[c], Elena Monfort[c], and James E. Wilhelm[a,c,*]

[a]Howard Hughes Medical Institute Summer Institute, Marine Biological Laboratory, Woods Hole, MA 02543; [b]Institute of Molecular Biosciences, Mahidol University, Phuttamonthon, Nakhon Pathom 73170, Thailand; [c]Division of Biological Sciences, University of California, San Diego, La Jolla, CA 92093

ABSTRACT **Despite the proliferation of proteins that can form filaments or phase-separated condensates, it remains unclear how this behavior is distributed over biological networks. We have found that 60 of the 440 yeast metabolic enzymes robustly form structures, including 10 that assemble within mitochondria. Additionally, the ability to assemble is enriched at branch points on several metabolic pathways. The assembly of enzymes at the first branch point in de novo purine biosynthesis is coordinated, hierarchical, and based on their position within the pathway, while the enzymes at the second branch point are recruited to RNA stress granules. Consistent with distinct classes of structures being deployed at different control points in a pathway, we find that the first enzyme in the pathway, PRPP synthetase, forms evolutionarily conserved filaments that are sequestered in the nucleus in higher eukaryotes. These findings provide a roadmap for identifying additional conserved features of metabolic regulation by condensates/filaments.**

Monitoring Editor
Laurent Blanchoin
CEA Grenoble

Received: Apr 23, 2019
Revised: Aug 2, 2019
Accepted: Aug 26, 2019

INTRODUCTION

One of the central problems of cell biology is how cells organize biochemical reactions in space and time. Traditionally, studies of this problem have focused on the compartmentalization of reactions within membrane compartments and organelles. Recently, however, there has been an increasing appreciation that the dynamic partitioning of proteins into novel nonmembranous compartments can be used to regulate cytoplasmic processes such as signal transduction and RNA metabolism (Banani *et al.*, 2017; Boeynaems *et al.*, 2018). While the interaction domains and biophysical principles that govern the assembly and disassembly of signaling microclusters and RNA granules are increasingly well understood (Ditlev *et al.*, 2018), it has remained unclear how this understanding might be deployed in other regulatory or biosynthetic networks.

Because many of the concepts, such as end-product inhibition, that we rely upon to understand how biological networks are regulated were first described in metabolism (Adelberg and Umbarger, 1953; Pardee and Yates, 1956; Gerhart and Pardee, 1962; Srere, 1987), one might expect that the formation of nonmembranous compartments may also play a critical role in regulating metabolic networks. Unfortunately, while studies have identified an increasing number of metabolic enzymes that are capable of forming biomolecular condensates and/or filaments, the connections between these structures and enzyme regulation have only been defined for a limited number of cases. For instance, end-product inhibition by CTP has been found to trigger polymerization of bacterial CTP synthetase in an inactive conformation (Barry *et al.*, 2014). Similarly, assembly of yeast glutamine synthetase results in its inactivation (Petrovska *et al.*, 2014). Conversely, work on mammalian CTP synthetase, mammalian acetyl CoA carboxylase, and liver phosphofructokinase has found that enzyme polymerization and activation are intimately connected (Meredith and Lane, 1978; Beaty and Lane, 1983a,b; Lynch *et al.*, 2017; Webb *et al.*, 2017). Thus, while metabolic enzyme filaments can be used to both activate and sequester enzymes, it remains

This article was published online ahead of print in MBoC in Press (http://www.molbiolcell.org/cgi/doi/10.1091/mbc.E19-04-0224) on September 4, 2019.

The authors declare no competing interests.

*Address correspondence to: James E. Wilhelm (jwilhelm@ucsd.edu).

Abbreviations used: CTP, cytidine 5′-triphosphate; GFP, green fluorescent protein; GTP, guanosine 5′-triphosphate; PBS, phosphate-buffered saline; PRPP, phosphoribosyl pyrophosphate; YPD, yeast extract-peptone-dextrose–containing medium.

unclear how such regulation is deployed throughout the metabolic network.

While the relationship between metabolites and higher-order enzyme assembly is best understood for metabolic enzyme filaments, it is clear that classes of metabolic enzymes can also form condensates that behave similarly to the phase-separated structures observed in RNA granules and signal transduction (Jang *et al.*, 2016; Banani *et al.*, 2017; Jin *et al.*, 2017). The fluid nature of these structures has also led to renewed interest in whether they could be used to facilitate substrate channeling by partitioning multiple enzymatic steps of a pathway into clusters (Srere, 1987). For instance, hypoxic stress has been found to trigger the reorganization of glycolytic enzymes in yeast and *Caenorhabditis elegans*, suggesting that clustering could enhance glycolytic activity in response to energy stress (Jang *et al.*, 2016; Jin *et al.*, 2017). Similarly, the enzymes in the mammalian de novo purine biosynthetic pathway condense into a single structure, the purinosome, in response to purine limitation, mTOR signaling, and mitochondrial dysfunction (An *et al.*, 2008, 2010; French *et al.*, 2016), but these results have been controversial due to their reliance on transient expression of fluorescently tagged proteins (Zhao *et al.*, 2013, 2014). Together, these findings suggest that distinct metabolic stresses can trigger sets of metabolic enzymes to form condensates via phase separation that can facilitate pathway flux. However, the basis of this phase-separating behavior and whether the assembly of entire pathways into a common structure is a broadly deployed mechanism for regulating metabolic networks remain open questions.

This lack of clarity is in spite of the fact that several biochemical and visual screens for proteins that form condensates and/or filaments have been conducted in *Saccharomyces cerevisiae* in recent years (Narayanaswamy *et al.*, 2009; Noree *et al.*, 2010; Tkach *et al.*, 2012; Mazumder *et al.*, 2013; O'Connell *et al.*, 2014; Chong *et al.*, 2015; Shen *et al.*, 2016). While these screens have greatly expanded the number of proteins that form structures, these studies have failed to identify any rules or principles that govern which metabolic enzymes can form condensates/filaments and which cannot. One possible reason for this failure is that the majority of visual screens have not quantitatively examined the frequency of structure formation across multiple growth conditions. Thus, enzymes that form structures in a small percentage of cells are on an equal footing with enzymes that robustly form structures in every cell, potentially complicating any analysis. Similarly, the fact that biochemical screens for protein aggregation detect only partial overlap with visual screens suggests that these two methodologies might have different levels of sensitivity for condensate/filament formation (O'Connell *et al.*, 2014). Thus, a screen that surveyed a variety of physiologically relevant growth conditions and measured the frequency of structure formation would provide a robust data set for understanding the relationship between pathway architecture and enzyme condensate/filament formation.

Additionally, previous screens have not explored the relationship between enzyme assembly and the known compartmentalization of biochemical pathways into organelles, such as mitochondria. Given the importance of pathway compartmentalization in regulating metabolic flux, determining which compartmentalized enzymes form structures and whether they assemble inside or outside the compartment could reveal missed connections between pathway architecture and the ability of enzymes to form condensates/filaments.

To address both of these issues, as well as to expand the repertoire of metabolic enzymes capable of forming structures, we measured the frequency at which all 440 proteins in the yeast green fluorescent protein (GFP) strain collection with an annotated role in metabolism form condensates/filaments under three different growth conditions (log phase, postdiauxic shift, and stationary phase). This screen identified 60 proteins capable of forming condensates or filaments in more than 10% of cells under at least one growth condition. This expanded the list of enzymes known to form condensates by 20. Our screen also identified 10 mitochondrial enzymes that form condensates within mitochondria at regions of high metabolic activity. Interestingly, we also identified several pathways where condensate formation was largely restricted to branch points in the metabolic network, suggesting that condensate formation might regulate flux at decision points in a pathway. Consistent with this, we found that the assembly of enzymes at the first branch point in de novo purine biosynthesis is coordinated, hierarchical, and based on their position within the pathway, while the enzymes at the second branch point are recruited to RNA stress granules. We have also found that the first enzyme in the pathway, phosphoribosyl pyrophosphate (PRPP) synthetase, forms evolutionarily conserved filaments that are sequestered in the nucleus in higher eukaryotes, arguing that while the ability to form structures may be conserved, the regulatory role of the structures may diverge. Together, these results provide a framework for understanding the variety of ways metabolic enzyme condensates and filaments can be used to regulate cellular metabolism.

RESULTS

A systematic screen for metabolic enzymes that form intracellular structures

Several screens to date have identified metabolic enzymes that assemble into intracellular structures (Narayanaswamy *et al.*, 2009; Noree *et al.*, 2010; O'Connell *et al.*, 2012, 2014; Tkach *et al.*, 2012; Mazumder *et al.*, 2013; Chong *et al.*, 2015; French *et al.*, 2016; Shen *et al.*, 2016; Saad *et al.*, 2017). However, many of these prior studies have focused on a single enzyme, pathway, or growth condition and often have scored only the presence or absence of a structure in the population of cells. This has made it difficult to determine how many metabolic enzymes are capable of assembly, the diversity of growth conditions that trigger assembly, and whether assembly occurs broadly or is restricted to a subpopulation of yeast cells.

The goal of our screen was to quantitatively assess the ability of all 440 metabolic enzymes to form structures under three different growth conditions: log phase, postdiauxic shift (1 d), and stationary phase (5 d; Figure 1A). Each of these growth conditions represents a distinct metabolic state. During log phase, yeast cells grow and divide rapidly by fermentation of glucose present in the medium. Upon glucose limitation, yeast enter the postdiauxic shift, where they grow slowly and use the ethanol they produced during log phase. After ethanol and other nutrients have been utilized, cell division is dramatically reduced and cells enter the stationary phase (Werner-Washburne *et al.*, 1993; Braun *et al.*, 1996).

By systematically identifying all of the enzymes that were capable of forming either foci or filaments and the frequency at which the structures formed, we hoped to identify any underlying principles governing which enzymes are capable of forming intracellular structures. Furthermore, because some GFP fusions cause aggregation in only a small percentage of cells, we included only enzymes that formed structures in more than 10% of cells in our analysis. By these criteria, our screen has identified 60 metabolic enzymes that formed structures in more than 10% of cells under at least one growth condition (Supplemental Table S1). Forty-seven of these metabolic enzymes formed focus-like structures, while 11

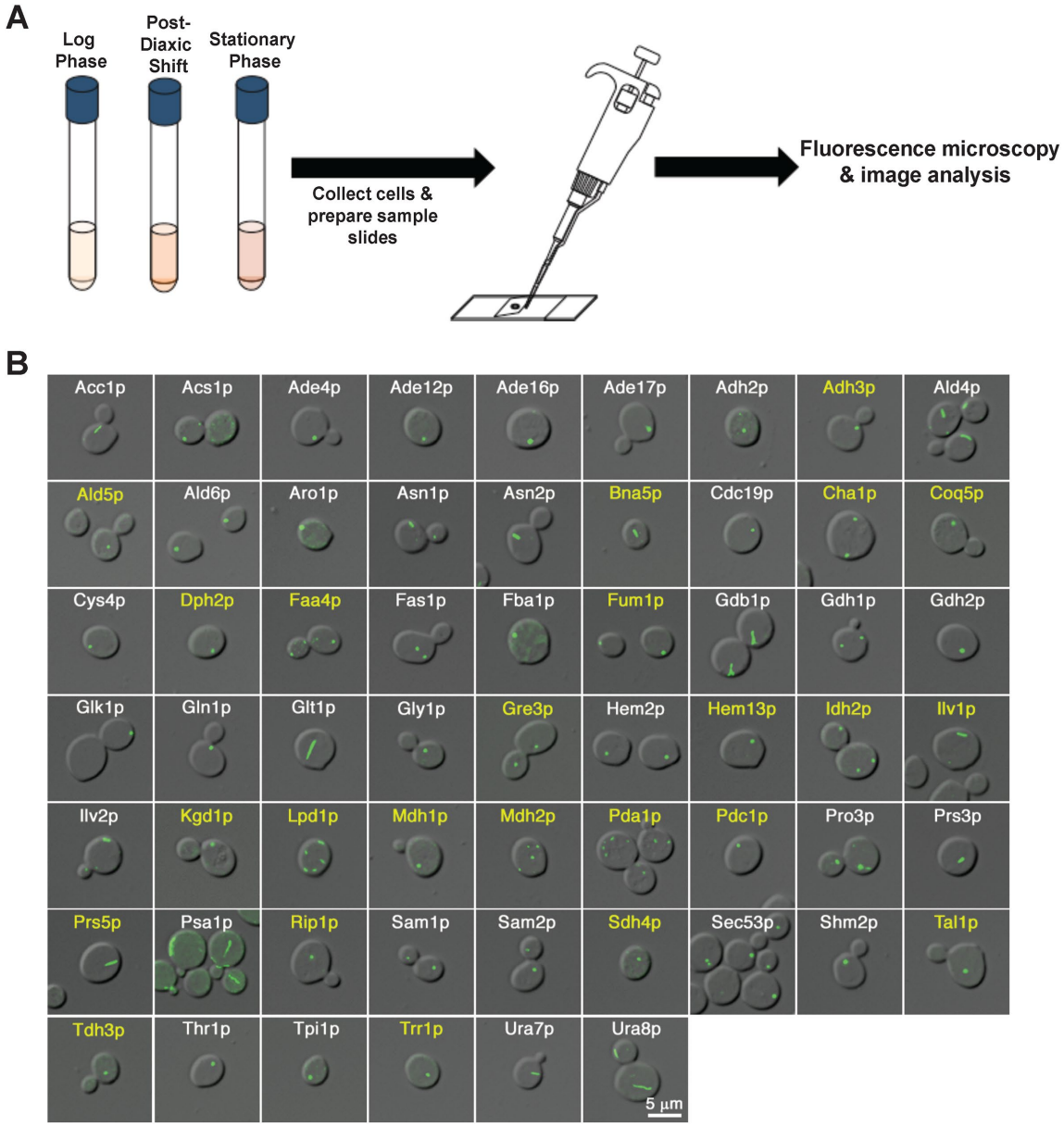

FIGURE 1: Screen of metabolic enzymes reveals 20 new proteins capable of assembly into foci or filaments. (A) Schematic for screening the yeast GFP collection to identify all metabolic enzymes with the ability to form structures. Each strain was grown to log phase, postdiauxic shift, and stationary phase in YPD and fixed in 4% formaldehyde at room temperature for 15 min. Cells were washed and resuspended in 1 M sorbitol before imaging. (B) Multiple growth conditions expand the list of metabolic enzymes forming assemblies. Representative images of metabolic enzymes capable of assembly into filaments or foci in more than 10% of cells. Enzyme names highlighted in yellow represent previously unknown metabolic enzymes forming assemblies. Images were taken from the culture condition with the highest degree of assembly.

assembled into discrete filaments (Figure 1B). Of these 11, we have identified three novel filament-forming enzymes that have not been identified in previous screens: Bna5p, Prs3p, and Prs5p. While Bna5 encodes for kynureninase, Prs3p and Prs5p are subunits of yeast PRPP synthetase. The remaining eight filament-forming enzymes were also identified in previous screens of the yeast GFP strain collection: acetyl CoA carboxylase (Acc1p), asparagine synthetase (Asn1p, Asn2p), glycogen debranching enzyme (Gdb1p), glutamate synthase (Glt1p), GDP-mannose pyrophosphorylase (Psa1p), and CTP synthetase (Ura7p, Ura8p; Noree *et al.*, 2010; Petrovska *et al.*, 2014; Shen *et al.*, 2016). While all of these enzymes are capable of forming distinct filaments, as assayed by pairwise colocalization (Supplemental Figure 1), five pairs of these filaments exhibit partial colocalization: Asn1p/Prs5p, Bna5p/Prs5p, Glt1p/Prs5p, Ura7p/Prs5p, and Gdb1p/Ura7p. This type of assembly is reminiscent of the stress-specific lateral assembly of CTP synthase filaments with IMP dehydrogenase filaments in mammalian cells (Carcamo *et al.*, 2011; Keppeke *et al.*, 2015; Chang *et al.*, 2018). Thus, in addition to identifying three novel filament-forming metabolic enzymes, our screen has also significantly increased the number of metabolic filaments capable of lateral interactions, providing a new window into this type of filament interaction.

Analysis of our screen revealed four basic patterns of assembly: log phase–restricted, stationary phase–restricted, nutrient-limited (restricted to both saturation and stationary phase), and constitutive. About 80% of the enzymes assemble solely when nutrients are limiting. The largest single category was enzymes that assembled during both saturation and stationary phase (26/59), followed closely by enzymes that assembled only in stationary phase (17/59). Thus, while nutrient limitation is a major trigger for assembly across all metabolic pathways, the type of nutrient limitation (postdiauxic shift vs. stationary) is a key determinant of whether a particular enzyme will assemble.

Identification of metabolic enzymes that form structures within mitochondria

Previous screens of the yeast GFP strain collection for novel intracellular structures have focused largely on the presence or absence of a structure. However, there has been no systematic assessment of whether these enzyme structures are associated with organelles or other structures in the cell. This is particularly problematic because the compartmentalization of several metabolic pathways to mitochondria is a key organizing principle of metabolic biochemistry. Furthermore, the yeast metabolic enzyme Ald4p has recently been found to form structures within the mitochondria, suggesting that a subset of metabolic enzymes might be forming within other compartments (Misonou *et al*., 2014; Noree, 2018). The fact that our screen identified 24 putative mitochondrial metabolic enzymes presented us with a unique opportunity to explore the extent of metabolic enzyme self-assembly within mitochondria. GFP yeast strains for each of the 24 hits from our screen with a mitochondrial annotation were stained with MitoTracker to determine whether the structures assembled inside or outside of mitochondria (Supplemental Table S1; Supplemental Figure 2). Ten of the enzymes formed discrete puncta within the mitochondria and had annotations where the sole localization reported in the SGD was the mitochondria (Figure 2A; Supplemental Figure 2). The remaining fourteen metabolic enzymes formed structures outside the mitochondria and were not studied further (Supplemental Figure 2).

In the course of analyzing our MitoTracker staining, we noted that enzyme structures were often found at sites of high signal. Because MitoTracker import reflects mitochondrial activity, this suggested that these enzymes were concentrated at regions of high respiratory activity. To confirm this, we also examined the localization of 10 assembling mitochondrial enzymes with the dye tetramethylrhodamine ethyl ester (TMRE), which, similarly to MitoTracker, displays brighter fluorescence signal at sites of high respiratory activity (Crowley *et al*., 2016). All 10 of these enzymes showed structure formation in regions of elevated mitochondrial activity with both dyes (Supplemental Figures 2 and 3). These results argued either that these enzymes were concentrated at regions of high respiratory activity or that enzymes accumulated at regions of high mitochondrial density. To distinguish between these two possibilities, we transformed a subset of our yeast GFP strains with a plasmid expressing dsRed fused to a mitochondrial targeting sequence. The distribution of these enzymes within the mitochondria was then examined under the growth conditions where foci formation is observed, either log phase (Ald4p) or postdiauxic shift (Fum1p, Ilv1p, Ilv2p). Our analysis revealed that the location of metabolic enzyme structures within mitochondria was not correlated with sites of high mitochondrial density, suggesting that these enzymes might be accumulating at sites of high mitochondrial activity (Figure 2B).

One potential location for these structures is the nucleoid, which has long been known to be associated with metabolic enzymes (Zelenaya-Troitskaya *et al*., 1995; Chen *et al*., 2007). However, the number of structures that we observe is not consistent with the typical numbers of nucleoids present within the mitochondrial network under these growth conditions (Miyakawa *et al*., 1984; Miyakawa, 2017). Furthermore, when we compared the results from our screen with proteomic analysis of the nucleoids from yeast, we found that only three of the 10 metabolic enzymes that copurified with nucleoids and were present in the GFP strain collection formed visible structures in our assay conditions (Miyakawa, 2017; Supplemental Figure 4). Thus, these enzymes are likely forming novel structures within mitochondria.

Enzymes that act at nodes in the purine biosynthetic pathway assemble into distinct visible intracellular structures

The fact that our screen uncovered interactions between different metabolic filaments and identified enzymes that assemble within mitochondria suggested that there might be levels of metabolic enzyme organization and coordination that have been missed in previous screens. To address this, we focused on one well-studied pathway, de novo purine biosynthesis, to determine whether there was any pattern to which enzymes formed structures and whether the pattern of assembly was coordinated with pathway activity/regulation. We chose to use the de novo purine biosynthesis pathway for two reasons. First, studies of the de novo purine biosynthetic pathway in mammals have identified a subset of enzymes assembled into a common structure in response to purine deprivation, the purinosome (Figure 3A; An *et al*., 2008). Second, while multiple purine biosynthetic enzymes in yeast have been found to form enzyme structures, the fact that these structures did not form a classic "purinosome" suggested that another form of regulation might be operating in *S. cerevisiae* (Narayanaswamy *et al*., 2009; O'Connell *et al*., 2014). Thus, a more in-depth analysis of this pathway in *S. cerevisiae* would allow us both to determine what aspects of enzyme organization, if any, are evolutionarily conserved and how assembly might be used to regulate metabolic flux through a pathway.

As part of this analysis, we rescreened all 21 proteins that compose the de novo purine biosynthetic pathway for the ability to assemble into intracellular structures, the frequency with which these structures form, and the growth conditions that triggered assembly, using the yeast GFP strain collection. For each enzyme, the percentage of cells with GFP-labeled structures was determined in triplicate for four different growth conditions: log phase growth and cultures grown to 1 d (postdiauxic shift), 3 d (transitional), or 5 d (stationary phase). Our quantitative analysis found that 12 of the 21 proteins involved in de novo purine biosynthesis displayed little if any assembly behavior (i.e., structures in <6% of cells under at least one growth condition; Figure 3, B–D; Supplemental Table S2). This list included Ade5,7p and Ade2p, which previous screens identified as forming foci (Narayanaswamy *et al*., 2009; O'Connell *et al*., 2014), but which form foci only at low frequency under our growth conditions (4.95% Ade5,7p; 2.98% Ade2p). In contrast, nine of the proteins showed a high level of assembly, with most forming structures in 30–80% of cells under at least one growth condition (Figure 3, B–D; Supplemental Table S2). These nine proteins that form structures represent five distinct purine biosynthetic enzymes: PRPP synthetase (Prs3p, Prs5p), PRPP amidotransferase (Ade4p), 5-amino-4-imidazolecarboxamide ribonucleotide transformylase/IMP cyclohydrolase (Ade16/17p), adenylosuccinate synthase (Ade12p), and inosine monophosphate (IMP) dehydrogenase (Imd2-4p). Interestingly, four

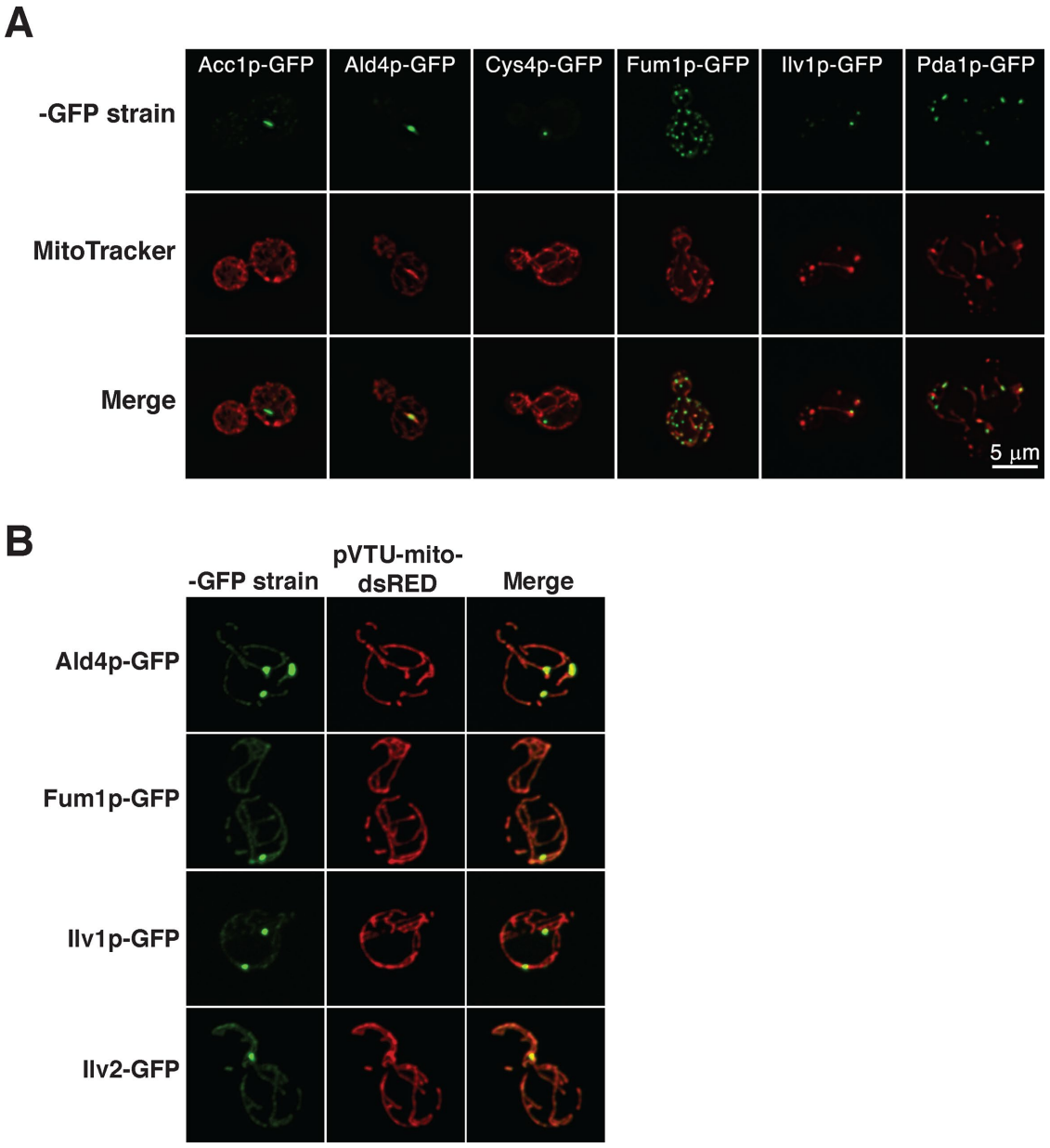

FIGURE 2: Metabolic enzymes can form discrete structures inside and/or outside of the mitochondria. (A) MitoTracker staining reveals differential distribution of metabolic enzyme structures inside or outside the mitochondria. Cells expressing GFP-tagged metabolic enzymes were incubated with 0.1 μM MitoTracker Red for 30 min. Cells were washed and then imaged immediately. (B) Assemblies of metabolic enzymes do not overlap with high-density regions of mitochondria. Cells expressing GFP-tagged metabolic enzymes were transformed with a plasmid containing a dsRed fluorescent protein attached to a mitochondrial targeting sequence (pVTU-mito-dsRED). Dual fluorescent strains were grown to either log phase (Ald4p) or postdiauxic shift (Fum1p, Ilv1p, Ilv2p) and imaged for colocalization.

of these five enzymes are known to be highly regulated by feedback inhibition and allosteric control, consistent with a role in flux control (Switzer and Sogin, 1973; Holmes *et al.*, 1974; Van der Weyden and Kelly, 1974; Wyngaarden, 1976; Smith, 1998; Rebora *et al.*, 2001). Additionally, all of these enzymes are found at branchpoints/nodes in the purine biosynthetic pathway. Furthermore, many enzymes that are recruited to the mammalian purinosome did not assemble to a significant degree in yeast. Using both HA and mNeonGreen fusions, we also confirmed that the assembly behavior of these nine proteins was not due to tag-specific dimerization or aggregation (Supplemental Figure 5). Additionally, the GFP tag did not cause auxotrophy in the cases where this could be examined (Supplemental Figure 5). Thus, these structures are not due to the GFP tag or protein denaturation.

The fact that these enzymes are assembling at branch points within a given pathway raised the question of whether or not this is a feature common to multiple metabolic pathways. Consistent with the de novo purine biosynthetic pathway, we found that enzymes that can form structures are found at highly connected portions of the glycolysis pathway, the glutamate biosynthetic pathway, and the methionine/cysteine biosynthetic pathway (Supplemental Figure 6). This suggests that spatial reorganization of metabolic enzymes might be used to coordinate flux through competing branches of particular pathways in response to nutrient limitation.

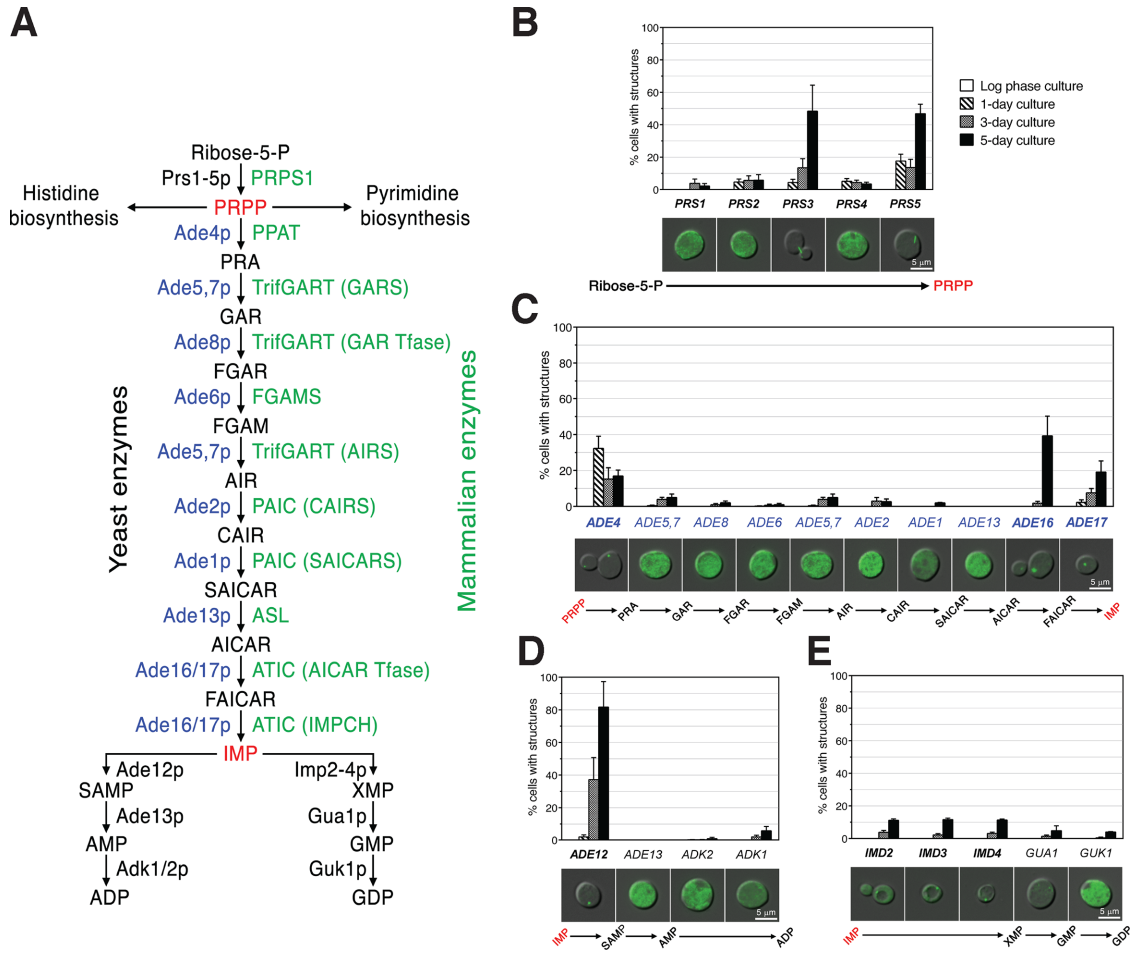

FIGURE 3: Enzymes in the de novo purine biosynthetic pathway assemble with different kinetics. (A) Schematic of the de novo purine biosynthetic pathway with yeast orthologues in blue on the left and mammalian orthologues in green on the right. Abbreviations for intermediate metabolites and catalytic enzymes: R5P = ribose-5-phosphate; PRPP = 5-phosphoribosylpyrophosphate; PRA = 5-phosphoribosylamine; GAR = 5-phosphoribosylglycineamide; FGAR = 5′-phosphoribosyl- *N*-formylglycinamide; FGAM = 5′-phosphoribosyl-*N*-formylglycinamidine; AIR = 5′-phosphoribosyl-5-aminoimidazole; CAIR = 5′- phosphoribosyl-4-carboxy-5-aminoimidazole; SAICAR = 5′-phosphoribosyl-4-(N-succinocarboxamide)-5-aminoimidazole; AICAR = 5-amino-4-imidazolecarboxamide ribotide; FAICAR = 5-formamido-1-(5-phosphoribosyl)-imidazole-4-carboxamide; IMP = inosine-5′-monophosphate; XMP = xanthosine-5′-phosphate; GMP = guanosine-5′-phosphate; GDP = guanosine-5′-diphosphate; SAMP = adenylosuccinate; AMP = adenosine-5′-phosphate; ADP = adenosine-5′-diphosphate; Prs1-5p = phosphoribosylpyrophosphate synthetase; Ade4p = amidophosphoribosyltransferase; Ade5,7p = GAR synthetase/AIR synthetase; Ade8p = GAR transformylase; Ade6p = FGAM synthetase; Ade2p = AIR carboxylase; Ade1p = SAICAR synthase; Ade16/17p = IMP cyclohydrolase; Ade12p = adenylosuccinate synthetase; Ade13p = adenylosuccinate lyase; Adk2p = mitochondrial GTP:AMP phosphotransferase; Adk1p = adenylate kinase; Imd2-4p = IMP dehydrogenase; Gua1p = GMP synthetase; Guk1p = guanylate kinase; PPAT = PRPP amidotransferase; TrifGART = trifunctional glycinamide ribonucleotide (GAR) transformylase; GARS = GAR synthase; GAR Tfase = GAR transformylase; AIRS = aminoimidazole ribonucleotide (AIR) synthase; FGAMS = formylglycinamidine ribonucleotide (FGAM) synthase; PAIC = phosphoribosylaminoimidazole carboxylase; CAIRS = carboxyaminoimidazole ribonucleotide (CAIR) synthase; SAICARS = succinylaminoimidazolecarboxamide ribonucleotide (SAICAR) synthase; ASL = adenylosuccinate lyase; ATIC = AICAR transformylase/IMP cyclohydrolase; AICAR Tfase = aminoimidazolecarboxamide ribonucleotide (AICAR) transformylase; IMPCH = IMP cyclohydrolase. (B) Assembly of PRPP synthetase subunits is enriched for Prs3p and Prs5p. GFP-tagged versions of the PRPP synthetase proteins (Prs1p, Prs2p, Prs3p, Prs4p, Prs5p) were grown in YPD to log phase, 1-, 3-, and 5-d time points and assayed for assembly formation. Representative images are shown below. (C) Only enzymes located at branch points (Ade4p and Ade16/17p) assemble into foci. GFP-tagged versions of purine biosynthetic enzymes acting in the middle of the pathway were grown under conditions identical to those indicated in B and assayed for assembly formation. Representative images are shown below. (D) Ade12p is the only enzyme forming foci in the ADP production branch. GFP-tagged versions of purine biosynthetic enzymes involved in ADP production were grown under conditions identical to those indicated in B and assayed for assembly formation. Representative images are shown below. (E) All subunits of the IMPDH complex assemble into foci. GFP-tagged versions of purine biosynthetic enzymes involved in GDP production were grown under conditions identical to those indicated in B and assayed for assembly formation. Representative images are shown below. Data are represented as means of at least three independent experiments; error bars indicate SEM. Images were taken from the culture condition with the highest degree of assembly.

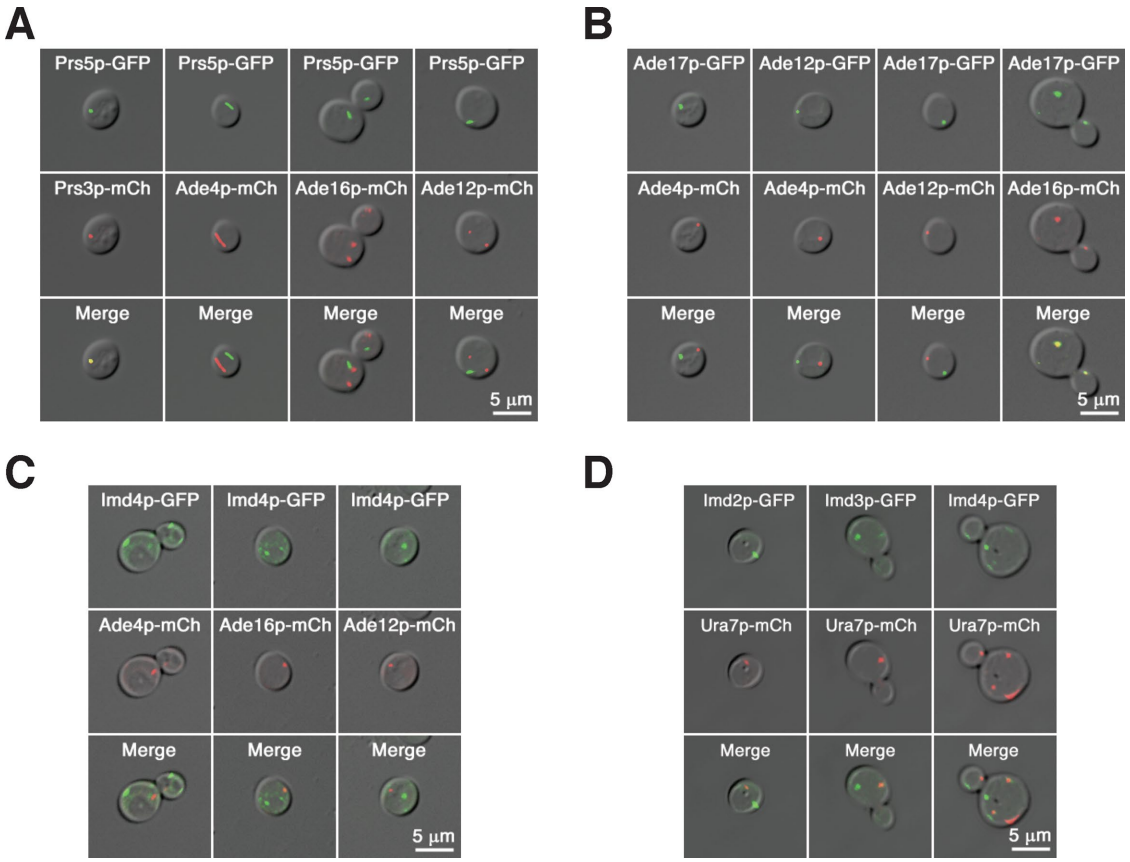

FIGURE 4: Only intracellular structures formed by metabolic enzymes performing the same reaction colocalize with each other. (A) Prs5p does not colocalize with any downstream enzyme in the de novo purine biosynthetic pathway. Dual fluorescent strains were grown to 5 d in YPD for imaging. (B) Only Ade16p and Ade17p foci show colocalization with each other. Growth conditions were identical to those indicated in A. (C) Imd4p fails to colocalize with its upstream enzyme (Ade4p, Ade16p) or its cross-pathway enzyme (Ade12p). Growth conditions were identical to those indicated in A. (D) Unlike in other eukaryotes, IMP dehydrogenase (Imd2-4p) does not colocalize with CTP synthetase (Ura7p). Growth conditions were identical to those indicated in A.

Higher-order assembly is not used for substrate channeling or to coordinate activity at distinct nodes

Our finding that the only enzymes that form structures at high frequency are those that act at nodes in the de novo purine biosynthetic pathway suggested three potential novel modes of regulation. First, the enzymes at nodes could coassemble to route products down specific pathways via substrate channeling. Second, the enzymes that act at different nodes could coassemble to facilitate feedback inhibition. Third, pathway flux might not be regulated via coassembly of enzymes in this pathway. To distinguish between these possibilities, we performed pairwise colocalization experiments between the enzymes that act at the first committed step in de novo purine biosynthesis (Prs3p, Prs5p, and Ade4p), as well as those that act at the second major branchpoint in the pathway, which are involved with generation and conversion of IMP into either GTP or ATP (Ade16p, Ade17p, Ade12p, and Imd4p). For each set of enzymes, one protein was tagged with GFP, while the second was tagged with mCherry (Figure 4). We observed colocalization only when enzymes acted at the same step: Prs3p and Prs5p (Figure 4A), which are both subunits of PRPP synthetase, and Ade16p and Ade17p, which are isozymes of the bifunctional 5-aminoimidazole-4-carboxamide ribonucleotide transformylase/IMP cyclohydrolase (Figure 4B). These results argue that the assembly of these enzymes into large structures is not a strategy for substrate channeling, since enzymes that act at different steps are not found in the same structure.

We next examined the possibility that enzymes acting at different nodes within the same or competing pathways might coassemble to facilitate coordinated regulation. First, we used pairwise colocalization experiments to determine whether any enzymes acted at the first decision point in de novo purine biosynthesis that coassembled with enzymes at the second decision point. Ade4p, which acts at the first committed step of de novo purine biosynthesis, showed no colocalization with any of the enzymes (Ade17p, Ade12p, and Imd4p) that act at the second decision point in the pathway (Figure 4C). Thus, the enzymes from the two major nodes of this pathway do not coassemble with each other. We also explored the possibility that enzymes that form intracellular structures and whose products are known to cross-regulate each other might coassemble to facilitate the balancing of flux through different parts of the metabolic network. Because the downstream products of Ade12p and Imd2/3/4p cross-regulate each other to ensure the balanced synthesis of ATP and GTP, we tested whether these enzymes coassemble to facilitate pathway balancing. We observed no colocalization of these enzymes, arguing that the formation of these structures is not necessary for coordinating the activity of the different branches of the de novo purine biosynthetic pathway (Figure 4C). We also extended this analysis to coordination between

purine and pyrimidine biosynthesis. Because CTP synthetase (Ura7p) is a highly studied metabolic polymer and is allosterically activated by GTP, the downstream product of Imd2/3/4p, we examined whether Ura7p and Imd2/3/4p structures colocalized (Levitzki and Koshland, 1972; Ingerson-Mahar *et al.*, 2010; Liu, 2010; Noree *et al.*, 2010; Carcamo *et al.*, 2011). Ura7p filaments were not associated with any of the structures formed by Imd2p, Imd3, or Imd4p (Figure 4D). Thus, while the ability of metabolic enzymes in the de novo purine biosynthetic pathway to form structures is restricted to those enzymes that act at key decision points in the pathway, there appears to be no coassembly to facilitate regulation within or between different pathways. This argues that the role of these enzyme structures in flux control does not occur via a substrate-channeling mechanism.

A subset of purine biosynthetic enzymes are components of RNA granules

Because the assembly of metabolic enzymes within the de novo purine biosynthetic pathway does not appear to be a mechanism for substrate channeling, we considered other ways these enzyme structures might impact metabolic flux. One way to control flux through a pathway is by modulating the levels of rate-limiting enzymes in the cytoplasm (Jin *et al.*, 2017; Saad *et al.*, 2017). It was recently shown that yeast pyruvate kinase, Cdc19p, was recruited into RNA granules upon carbon starvation to regulate its enzymatic activity, highlighting a new localization pattern for controlling metabolic flux (Saad *et al.*, 2017). Because many RNA granules form in the cytoplasm under the same conditions that cause metabolic enzymes to assemble, we examined the possibility of any purine biosynthetic enzymes having similar cross-talk with these structures. To explore this possibility, we tested whether enzymes in purine biosynthesis form structures colocalized with RNA stress granules (Ded1p-mCherry) and/or processing bodies (Edc3p-mCherry). Prs3p and Prs5p were excluded from these studies because they form filaments that are clearly distinct from RNA granules. While Ade4p and Ade12p showed little (<5%) localization with either RNA granule marker when yeast is grown to stationary phase, the vast majority of Ade16p (91%) and Ade17p (90%) colocalized with the stress granule marker, Ded1p (Figure 5A; Supplemental Table S3). Furthermore, the remaining Ade16p (8%) and Ade17p (9%) structures appear to be processing bodies, as measured by colocalization with the processing body marker Edc3p-mCherry (Figure 5B; Supplemental Table S3). Thus, while stationary phase is a trigger for all four enzymes to assemble, only Ade16/17p is specifically recruited to RNA granules.

We also observed a higher degree of colocalization of Imd3p with stress granules than of Imd2p of Imd4p (Figure 5, A and B; Supplemental Table S3). The recruitment of one isoform of IMP dehydrogenase to stress granules suggests that Imd3p possesses a potential novel function in RNA metabolism, whereas the other isoforms do not. To further validate the presence of metabolic enzymes in stress granules, we assessed the degree of colocalization of Ade16p foci with two stress granule–associated chaperones, Hsp104p (69%) and Ssa1p (21%; Figure 5, C–E; Supplemental Table S4). Surprisingly, Ade16/17p and Imd3p also lack the prion-like/low-complexity domains that typically play a role in recruitment of proteins to stress granules, suggesting that they are recruited via a novel mechanism (Protter and Parker, 2016). Thus, Ade16/17p and Imd3p are novel components of stress granules and their association suggests a potential role in posttranscriptional gene regulation and metabolism.

Specific subunits of PRPP synthetase polymerize under distinct growth conditions

Because only a subset of purine enzymes are localized to RNA granules, we next explored other mechanisms for controlling pathway activity, such as the sequestration of essential subunits into a structure. Yeast PRPP synthetase presents an excellent case study for such a possibility, due to its unusual subunit architecture. While PRPP synthetases in other organisms are homooligomeric, no single yeast Prs protein can form a functional enzyme and only certain heterooligomeric combinations of the five Prs proteins are enzymatically active. Our initial screen identified two subunits (Prs3p and Prs5p) that were capable of filament formation and colocalized to the same structure (Figure 4A). Interestingly, all of the enzymatically active combinations of Prs subunits contain either Prs3p or Prs5p, but not both. Thus, these two subunits appear to delineate distinct forms of PRPP synthetase, a conclusion that is supported by the fact that *PRS3*Δ and *PRS5*Δ are synthetically lethal with each other (Hernando *et al.*, 1998, 1999).

If selective polymerization of Prs3p and Prs5p is a mechanism for regulating PRPP synthetase activity, we would expect that the assembly/disassembly of each subunit might be triggered by distinct growth conditions. To test this, we examined whether a brief 30-min shift into fresh medium could trigger the disassembly of Prs3p and/or Prs5p filaments in yeast grown to stationary phase. This shift caused the rapid disassembly of both Prs3p and Prs5p filaments, while the protein levels of both proteins remained constant. Furthermore, 30-min shifts to YP alone caused no disassembly of Prs3p and Prs5p filaments (Figure 6A; Supplemental Table S5). As a result, we focused our attention on the role of glucose in triggering disassembly of these filaments. Both Prs3p and Prs5p filaments disassemble in response to either the addition of fresh glucose to the culture or a 30-min shift to 2% glucose. Thus, the disassembly of both types of filaments is regulated by glucose.

Because addition of glucose triggers disassembly of Prs3p and Prs5p filaments, we predicted that removal of glucose from log-phase cultures would trigger assembly. Interestingly, the assembly of Prs3p and Prs5p showed a differential response to glucose removal. While Prs3 and Prs5 do not show any structures during logarithmic growth, a 30-min shift to a medium lacking glucose was sufficient to trigger Prs5p filament formation in ~90% of cells, but did not trigger Prs3p assembly (Figure 6B; Supplemental Table S6). Thus, two different subunits of PRPP synthetase in yeast, Prs5p and Prs3p, form filaments under distinct conditions: Prs3p assembles only in stationary phase, while Prs5p assembles in response to acute glucose limitation and stationary phase. Because glucose can directly generate the substrate for PRPP synthetase, ribose-5-phosphate, via the pentose phosphate pathway (Zimmer, 1992), this result suggests that substrate availability could regulate polymerization of Prs3p and Prs5p.

Ade4p assembly is regulated by end-product inhibition

Given our results with PRPP synthetase, we next examined the disassembly behavior of the other purine biosynthetic enzymes that form structures. In all cases, a brief 30-min shift to fresh YPD caused elimination of all of the structures with no change in protein level (Figure 6A; Supplemental Figure 7). Additionally, shifting to YP had little or no effect on the disassembly of any of the purine biosynthetic structures (Figure 6A; Supplemental Figure 7; Supplemental Table S5). This suggested that glucose might regulate the disassembly of all of the structures in the de novo purine biosynthetic pathway. The addition of fresh glucose to the culture or a 30-min shift to 2% glucose caused Ade16/17p, Ade12p, and

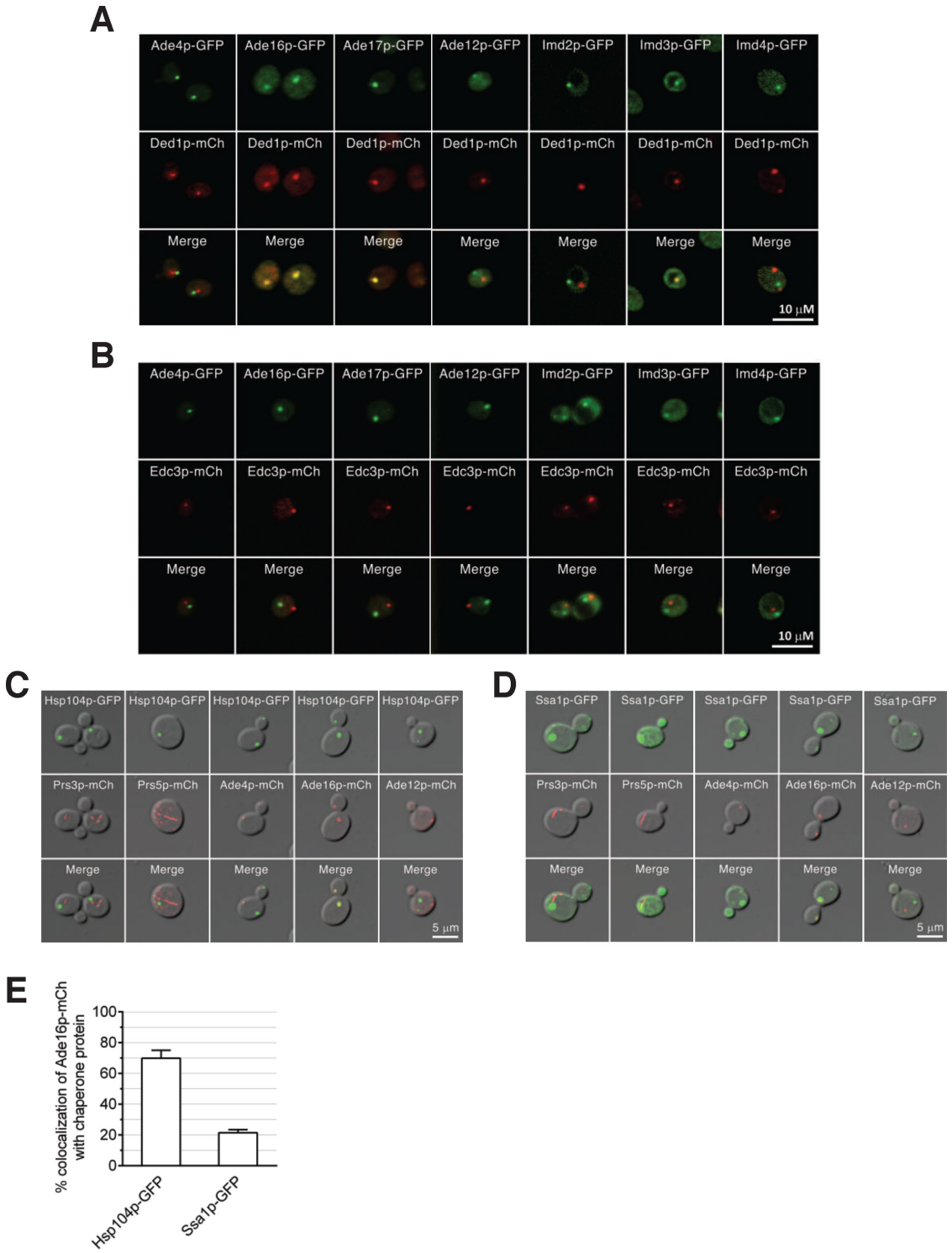

FIGURE 5: Ade16p, Ade17p, and Imd3p are recruited into stress granules. (A) Ade16p, Ade17p, and Imd3p display high levels of colocalization with the stress granule marker Ded1p. Dual fluorescent strains were grown in YPD to 5 d, with the exception of Ade4p-GFP, which was examined at 1 d. (B) Enzymes in the purine biosynthetic pathway showed no colocalization with the processing body marker Edc3p. Growth conditions were identical to those indicated in A. (C) Ade16p colocalizes with the known stress granule–associated chaperone Hsp104p. Growth conditions were identical to those indicated in A. (D) Ade16p colocalizes with the known stress granule–associated chaperone Ssa1p. Growth conditions were identical to those indicated in A. (E) Quantification of colocalization of Ade16p with the chaperones Hsp104p and Ssa1p. Data are represented as means of at least three independent experiments; error bars indicate SEM.

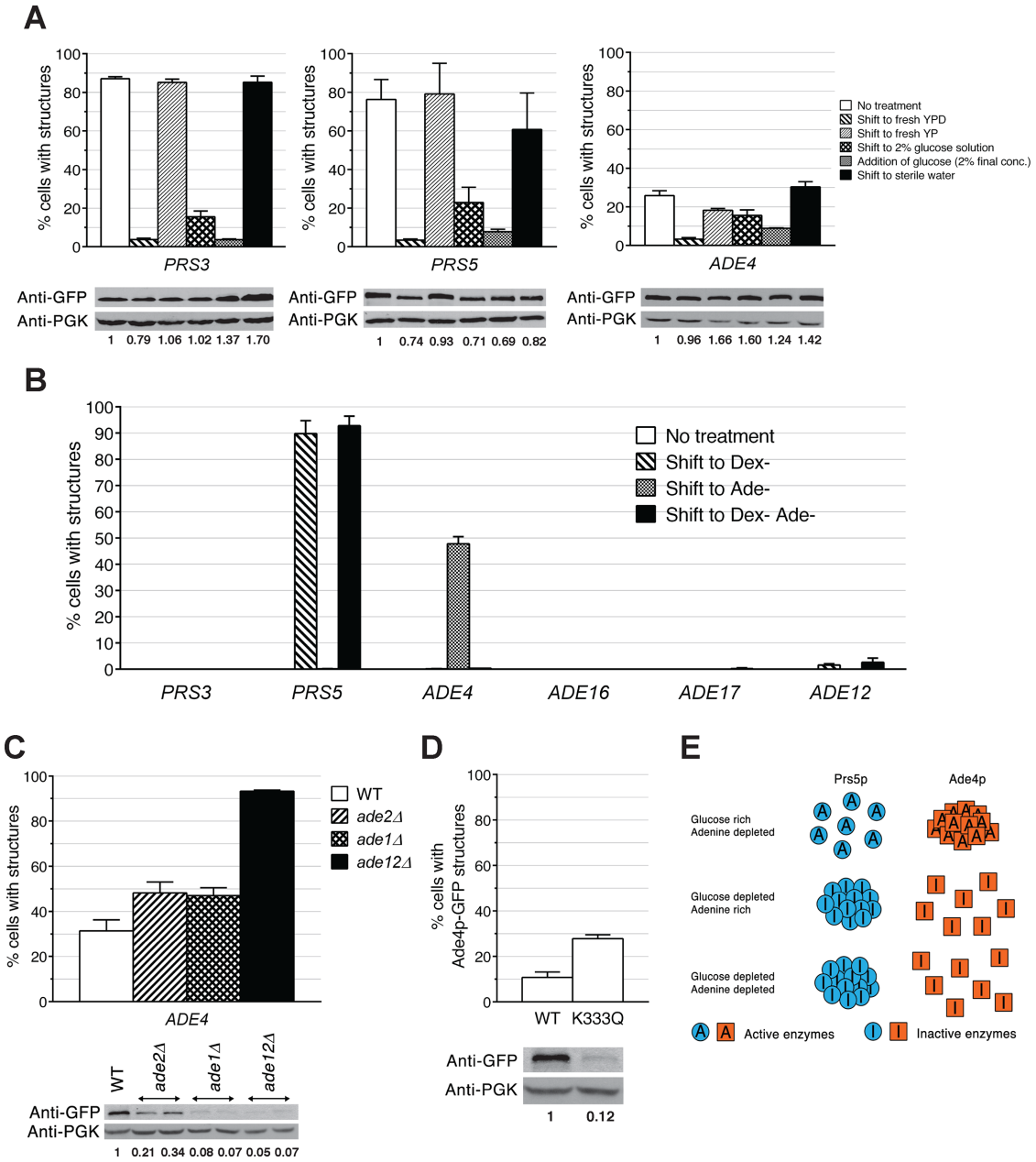

FIGURE 6: Coordinated structure formation of Prs5p and Ade4p controls pathway flux. (A) Prs3p, Prs5p, and Ade4p structures disassemble in response to the presence of fresh glucose. Cells expressing GFP-tagged purine biosynthetic enzymes were grown in YPD for 5 d, except for the *ADE4::GFP* strain (1 d), and then shifted into the indicated media, incubated for 30 min at 30°C, and visualized immediately. Protein levels were determined by Western blot analysis and were normalized to no- treatment samples (indicated below blots). (B) Prs5p and Ade4p have distinct triggers for structure formation. Yeast cells expressing GFP-tagged purine biosynthetic enzymes were grown to log phase in complete SD media, shifted into the indicated media for 30 min at 30°C, and counted immediately. (C) Deletion of downstream enzymes of Ade4p leads to increased structure formation of Ade4p. Wild-type and mutant cells expressing Ade4p-GFP were grown in YPD for 1 d at 30°C and scored for structure formation. Protein levels were determined by Western blot analysis and were normalized to the wild-type strain (indicated below blots). (D) Loss of feedback inhibition increases focus formation by Ade4p. Cells expressing wild-type Ade4p-GFP and Ade4p(K333Q)-GFP were grown to log phase in YPD and cells were scored for frequency of structure formation. Protein levels were determined by Western blot analysis and were normalized to the wild-type strain (indicated below blots). Data are represented as means of at least three independent experiments; error bars indicate SEM. (E) Model for the coordinating activity of Prs5p and Ade4p with regulated structure assembly statuses is illustrated.

Imd2-4p structures to disassemble without a change in protein level (Supplemental Figure 7); however, Ade4p structures remained intact (Figure 6; Supplemental Table S5). Additionally, we found that acute removal of glucose does not trigger the assembly of any purine biosynthetic enzyme other than Prs5p (Figure 6B). Thus, only Prs5p and Ade4p structures showed assembly/disassembly behavior that was distinct from that of the other enzymes in the pathway.

Given this result, we focused our attention on whether acute removal of adenine from the growth medium could trigger purine biosynthetic enzymes to assemble. We focused on the response to adenine limitation for two reasons. First, adenine removal would be predicted to increase flux though the de novo purine biosynthetic pathway. Thus, enzymes that assemble would be likely to be doing so in response to increased activity. Second, recent work on Ade4p suggested that removal of adenine for 2 h caused Ade4p to assemble into structures in a translation-dependent manner, raising the possibility that Ade4p structures form due to increased protein levels in response to adenine deprivation (Narayanaswamy *et al.*, 2009; O'Connell *et al.*, 2014). To identify purine biosynthetic enzymes that formed adenine-responsive structures, strains were grown to log phase and then shifted to Ade– media for 30 min. Only Ade4p assembled (48% of cells), and no change in Ade4p protein levels was observed (Figure 6B; Supplemental Table S6). These results suggested that Ade4p formed structures in response to increased enzyme/pathway activity.

While adenine removal is a potent driver of Ade4p assembly, it was unclear what metabolic changes might be triggering the assembly of Ade4p structures. Transcription of purine biosynthetic genes is known to increase in response to the elevated levels of the metabolic intermediate 5-aminoimidazole-4-carboxamide ribonucleotide (AICAR) that occur when flux through the pathway decreases (Pinson *et al.*, 2009). To explore whether Ade4p assembly might be responding to changes in metabolite levels, we assayed the effect of deleting different enzymes in de novo purine biosynthesis on the assembly of Ade4p foci. Interestingly, Ade4p assembly differed from the transcriptional regulation of the *ADE* genes in that deletion of enzymes that act upstream of AICAR biosynthesis (*ADE1* and *ADE2*), as well as of those that act downstream (*ADE12*), increased the number of Ade4p foci when cultures were grown to 1 d (Rebora *et al.*, 2001; Pinson *et al.*, 2009; Figure 6C). While all three deletions caused an increase in Ade4p foci as compared with wild type, the magnitude of the response differed between the different mutations. Deletion of either *ADE1* or *ADE2* caused a 1.5-fold increase in Ade4p foci as compared with wild type, while deletion of *ADE12*, which acts downstream of IMP biosynthesis, caused a threefold increase in Ade4p foci with almost all cells (93%) possessing Ade4p structures (Figure 6C; Supplemental Table S7). Notably, the increase in Ade4p focus formation occurred even though deletion of *ADE1, ADE2,* or *ADE12* causes a decrease in Ade4p protein levels. The fact that disruption of either ATP and GTP synthesis (*ade1*Δ and *ade2*Δ) or solely ATP synthesis (*ade12*Δ) triggers an increase in Ade4p structures independent of expression levels suggested that decreases and/or imbalances in the amount of end products of the pathway regulate Ade4p assembly. Our epistasis analysis of Ade4p assembly is also consistent with the fact that Ade4p activity is regulated by ATP and/or GTP levels via a feedback inhibition mechanism (Rebora *et al.*, 2001).

To investigate whether Ade4p focus formation is responsive to feedback inhibition, we leveraged previous structural and biochemical studies of *Escherichia coli* amidophosphoribosyltransferase, the orthologue of Ade4p, which identified K326Q as a mutation that confers resistance to feedback inhibition without affecting enzyme activity (Zhou *et al.*, 1993). To assess the role of feedback inhibition in Ade4p assembly, we introduced the equivalent mutation (K333Q) into the chromosomal *ADE4* gene in yeast and measured the frequency of structure formation in log phase for Ade4p(K333Q)-GFP as compared with wild-type cells. The Ade4p(K333Q)-GFP strain displayed a 2.6-fold increase in the percentage of cells with structures as compared with wild type, consistent with increased enzyme activity driving Ade4p assembly (Figure 6D; Supplemental Table S8). Thus, while Prs5p subunits are sequestered in an inactive filament, Ade4p assembles under conditions that either decrease end-product inhibition or necessitate increased pathway flux.

The assembly of Ade4p and Prs5p is coordinately regulated

If the ability of metabolic enzymes to assemble into filaments and foci is a mechanism for controlling pathway flux, one would expect that assembly/disassembly of different enzymes in the same pathway would be highly coordinated. Consistent with this, we have found that acute glucose removal triggers down-regulation of PRPP synthetase activity via Prs5p sequestration, but does not cause activation of Ade4p and the assembly of Ade4p into structures (Figure 6, A and B). Interestingly, the converse is also true—acute adenine removal causes activation of Ade4p and the formation of Ade4p structures, but does not cause the inactivation of PRPP synthetase by Prs5p polymerization (Figure 6B). While these observations are consistent with coordinated regulation of enzyme assembly, regulation of assembly via glucose and adenine could be occurring independent of each other. If Prs5p polymerization and Ade4p assembly were truly coordinately regulated, one would predict that removal of both glucose and adenine would cause Prs5p to assemble and would block the assembly of Ade4p. This is because there is no reason to activate Ade4p, even in the absence of adenine, if the upstream enzymes are inactivated or down-regulated. Consistent with this prediction, only Prs5p forms structures when yeast are shifted to media lacking both glucose and adenine (Figure 6B). Thus, the assembly of Prs5p and Ade4p is coordinately regulated and the hierarchy of assembly reflects their relative position in the de novo purine biosynthetic pathway (Figure 6E).

The assembly of PRPP synthetase is evolutionarily conserved

The coordinate regulation of Prs5p and Ade4p assembly raised the question of whether the ability of these enzymes to form structures is evolutionarily conserved. Previous work on the mammalian orthologue of Ade4p, PPAT, found that it was recruited to purinosomes in response to purine deprivation (An *et al.*, 2008). This suggested that activation of PPAT/Ade4p via recruitment to an intracellular structure might be evolutionarily conserved. However, the unusual subunit architecture of yeast PRPP synthetase suggested that polymerization might be unique to the yeast enzyme. The active forms of yeast PRPP synthetase are assembled from unique combinations of the 5 *PRS* gene products (Hove-Jensen, 2004). This allows the potential down-regulation of enzyme activity by sequestering an essential subunit via polymerization. However, mammalian PRPP synthetases are homohexameric, suggesting that this type of regulation might not exist in higher eukaryotes (Li *et al.*, 2007). To test whether the PRPP synthetase filament formation is evolutionarily conserved, we immunostained *Drosophila* ovaries, rat hippocampal neurons, and human primary culture fibroblasts for PRPP synthetase. In all three cases, we found that PRPP synthetase forms filaments in the nucleus under normal growth conditions (Figure 7, A–C). Thus, the ability of PRPP synthetase to form filaments is evolutionarily conserved.

DISCUSSION

Regulation of metabolic networks by self-assembling enzymes

There have been several proposed roles for metabolic enzymes assembling into supramolecular complexes. End-product inhibition by CTP is a trigger for bacterial CTP synthetase to polymerize in an

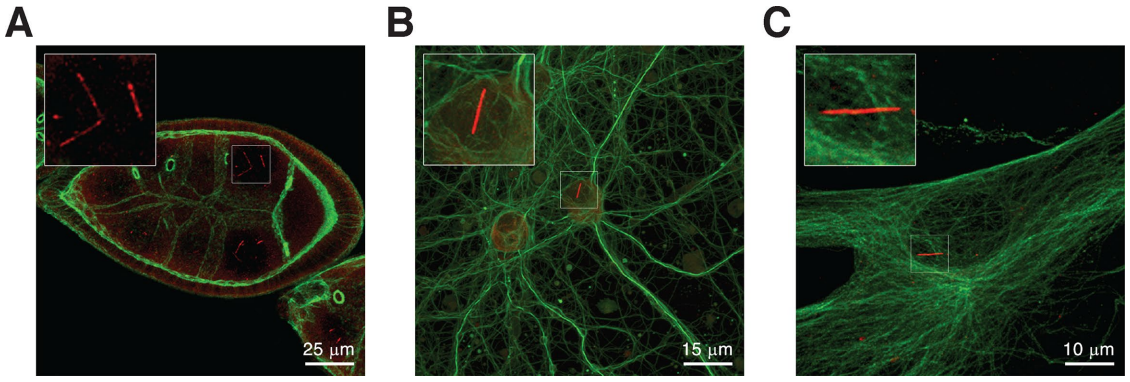

FIGURE 7: Filament formation of PRPP synthetase is evolutionarily conserved. Conservation of PRPP synthetase into filaments observed in *Drosophila* egg chambers (A), rat neurons (B), and human fibroblasts (C). The insert at the top left corner of each image is 3× magnified from the original image. PRPP synthase is stained with anti-PRPS1 (Covance; in red), and tubulin is detected with anti–tubulin-FITC (Sigma; in green).

inactive state, arguing that the formation of these complexes can be used to buffer the amount of free, active enzyme (Barry *et al.*, 2014). In contrast, acetyl Co-A carboxylase forms filaments as part of its activation mechanism, arguing that polymerization might facilitate cooperative activation of the enzyme (Meredith and Lane, 1978; Beaty and Lane, 1983b). In addition to playing roles in activation and inactivation of single enzymes, multiple enzymes of the mammalian de novo purine biosynthetic pathway coassemble into a single structure, the purinosome, which argues that these structures might also play a role in accelerating pathway flux via substrate channeling (An *et al.*, 2008). While these studies have supported a variety of regulatory roles for metabolic enzyme structures, it has remained unclear whether this type of regulation is just an idiosyncratic feature of particular enzymes or there are rules that determine where in a metabolic network this type of regulation is deployed.

Our visual screen of the yeast GFP strain collection identified 60 metabolic enzymes that are capable of forming structures. In contrast to other previous screens of the yeast GFP strain collection, we assayed multiple growth conditions and measured the extent of structure formation in the population of cells. Our analysis revealed that assembly of metabolic enzymes was often associated with locations within a pathway where either their substrate or their product is highly connected with other parts of the metabolic network. This selective positioning could be important in times of growth and stress, where reorganization of enzymes could promote and inactivate enzyme activity to ensure coordination of metabolites.

This conclusion is supported by our analysis of Prs5p and Ade4p assembly in the de novo purine biosynthetic pathway. If enzyme polymerization/assembly were a mechanism for controlling pathway activity, we would expect the formation of these structures to be coordinately regulated—there is no need to activate a downstream enzyme if the upstream enzymes have been inactivated. The fact that the assembly of Prs5p into an inactive polymer occurs when glucose is limiting, while the Ade4p foci form when the pathway is activated in response to a lack of adenine, provided a unique opportunity to test this mechanism of pathway regulation. Our observation that when yeast is acutely deprived of both glucose and adenine, Prs5p polymerizes, while Ade4p remains dispersed within the cytoplasm, argues that these structures are coordinately controlled and that there is a hierarchy to their formation: inactivation of upstream steps (Prs5p filament formation) blocks the activation of downstream steps (Ade4p foci formation).

This result also has implications for recent studies of the effect of nutrient limitation, ATP depletion, and pH on cytoplasmic fluidity and crowding. It has been proposed that each of these factors can drive the assembly of protein condensate filaments via its effect on cell volume, protein solubility, and/or cytoplasmic fluidity (Petrovska *et al.*, 2014; Joyner *et al.*, 2016; Munder *et al.*, 2016). The behavior of Prs5p and Ade4p, however, suggests that there is not a single biophysical signal triggering enzymes to form condensates and/or filaments. Most likely, these biophysical signals sensitize the system and facilitate metabolic enzyme assembly in response to specific nutrient states, such as glucose and/or adenine depletion.

Previous reports have supported the notion that assembly of consecutive enzymes in a metabolic pathway acts to facilitate flux through a pathway via substrate channeling. However, we found little support for substrate channeling from our screen. Consistent with the lack of a yeast equivalent of the mammalian purinosome, our global analysis did not identify entire pathways composed of enzymes that formed structures. This was particularly true in glycolysis, where we found that none of the enzymes that form structures act at consecutive steps of the pathway. Instead, the glycolytic enzymes that were capable of assembly either generated or consumed highly connected metabolites in the pathway. Given that many of the intermediates derived from glycolysis fuel other pathways such as amino acid or lipid biosynthesis, the assembly of a subset of glycolytic enzymes into these structures may provide a mechanism for efficient utilization of carbon sources by gating flux through multiple branching pathways. Furthermore, the set of glycolytic enzymes that form structures may be adaptive to specific stresses, since the enzymes we identified do not substantially overlap with those found to be localized to RNA granules in response to hypoxic stress (Jin *et al.*, 2017).

Stress granules and filaments as potential sites of metabolic enzyme cross-regulation

Interestingly, while we find little evidence for assembly of enzymes acting in consecutive steps of a metabolic pathway, we did find limited colocalization of enzymes in different pathways in two situations we examined. First, we found five pairs of metabolic enzyme filaments (Supplemental Figure 1) that interacted with each other in addition to forming separate filaments. Interestingly, before our screen, only two metabolic enzyme filaments were known to interact with each other: IMP dehydrogenase and CTP synthetase. The lateral interaction between these two enzyme filaments in response

to specific stresses has been proposed to help balance CTP and GTP biosynthesis in mammals (Carcamo *et al.*, 2011; Liu, 2016). However, we found that this interaction is not conserved because none of the IMP dehydrogenases (Imp2-4p) in yeast form filaments. Interestingly, filaments composed of the yeast CTP synthetase, Ura7p, do interact with filaments composed of the Prs5p subunit of PRPP synthetase. The interaction between filaments composed of enzymes that act at the top of purine biosynthesis and the bottom of pyrimidine biosynthesis suggests that the regulatory possibilities proposed for IMPDH and CTPS in mammals might also occur in yeast, but with different sets of enzymes. While the potential regulatory interactions between the remaining pairs of interacting filaments remains unclear, the results of our screen provide a basis for future studies for defining the structural basis for how distinct enzyme filaments can interact.

Ironically, the other example of enzyme colocalization that we observed was yeast IMP dehydrogenase coassembling with two other enzymes that act at the second branch point of the de novo purine biosynthetic pathway. Instead of forming autonomous structures such as Prs5 and Ade4, these three enzymes are recruited into stress granules. This observation suggests that recruitment of IMP dehydrogenase into enzyme regulatory structures might be a recurring theme in evolution, but that the nature of the structure (filament vs. stress granule) may vary from species to species. Additionally, the localization of metabolic enzymes in stress granules suggests that not all metabolic enzyme structures are composed solely of metabolic enzymes and that they could play roles in integrating metabolic regulation with the control of other cellular pathways. This is consistent with the role of RNA granules in recruiting and regulating the activity of particular signaling pathways (Shah *et al.*, 2014; Zhang *et al.*, 2016). Given that the identity of which glycolytic enzymes are recruited into RNA granules varies depending on the stress, it is possible that RNA granule recruitment provides a route for differentially regulating metabolic pathways in response to translational, oxidative, and/or nutrient stresses (Jin *et al.*, 2017).

Alternatively, there has been increasing interest in the possibility that certain metabolic enzymes can act as RNA-binding proteins to regulate gene expression posttranscriptionally. This interest has been driven by results from global screens for RNA-binding proteins that identified a large number of metabolic enzymes, as well as previous studies of the TCA cycle enzyme aconitase (Scherrer *et al.*, 2010; Castello *et al.*, 2012, 2016; Mitchell *et al.*, 2013; Liao *et al.*, 2016). Aconitase is an Fe–S cluster enzyme; however, when iron limitation leads to failure to form an Fe–S cluster, it is an RNA-binding protein that regulates the translation and stability of mRNAs for key iron uptake genes, such as transferrin (Haile *et al.*, 1992; Eisenstein, 2000). While only Imd3p has been identified as a RNA-binding protein in global screens, the localization of these three purine biosynthetic enzymes in stress granules implies that they could have secondary functions similar to those of other moonlighting enzymes such as aconitase (Mitchell *et al.*, 2013). Future studies directed at identifying the complete set of metabolic enzymes that localize in stress granules will help determine whether stress granules act as sites for integrating stress response with metabolic activity or whether the localization reflects additional moonlighting roles for a subset of metabolic enzymes.

Conservation of metabolic enzyme assembly

CTP synthetase filament formation was simultaneously discovered in bacteria, *Drosophila melanogaster*, *S. cerevisiae*, and humans (Ingerson-Mahar *et al.*, 2010; Liu, 2010; Noree *et al.*, 2010; Carcamo *et al.*, 2011). This suggested that the ability of metabolic enzymes to assemble into structures might be broadly conserved across species. However, the fact that the purinosome is not conserved from yeast to mammals argued that there may not be a simple one-to-one correspondence between enzyme structures in different species. The results of our screen provide a robust foundation for comparing assembly behavior across species. For instance, our screen identified 10 metabolic enzymes that form structures within mitochondria. These 10 metabolic enzyme structures do not appear to be localized in nucleoids or other known mitochondrial structures, based on their distribution. While the sole purpose of these structures could be to regulate enzyme activity, it is also possible that these structures could play a role in organizing the numerous membrane contacts between mitochondria and other organelles (Lackner, 2019). Alternatively, they could play a role in partitioning metabolic activity throughout the mitochondrial reticulum—a result consistent with our finding that enzyme structures are found in the mitochondrial regions with the highest metabolic activity (Figure 2; Supplemental Figures 2 and 3). Determining whether these 10 enzymes form structures in the mitochondria of higher eukaryotes and/or bacteria could help address these questions as well as providing insights into how metabolic enzyme assembly can be coopted by evolution to solve different biological problems.

One example of this approach is evidenced by our discovery that the ability of PRPP synthetase to form filaments is conserved from yeast to humans. Furthermore, our observation that PRPP synthetase forms filaments in the nuclei of mammalian cells, while in *S. cerevisiae*, the filaments are composed of inactive subunits that polymerize in the cytoplasm, argues that assembly might be conserved, but the purpose and location of the structure may vary greatly between species. Given that many inborn errors in metabolism display tissue-specific phenotypes that are difficult to explain in light of the known biochemical function of the enzyme, future comparative studies that leverage the results of our screen could provide insights into whether enzyme assembly behavior contributes to the pathophysiology of some of these diseases.

MATERIALS AND METHODS

Yeast strains and media

Yeast strains used in this study are listed in Supplemental Table S9. Briefly, all strains were grown at 30°C in 5 ml liquid YPD (2% peptone, 1% yeast extract, 2% dextrose) unless otherwise indicated, with shaking for the indicated time points. Strains with GFP-tagged proteins were from the yeast GFP collection (Howson *et al.*, 2005).

Yeast GFP collection screen

Cells were fixed by adding 100 µl of 37% wt/vol formaldehyde to 1 ml of yeast liquid culture and incubated on a rotating platform for at least 15 min at room temperature. Cells were then washed once with sterile water and resuspended in 1 M sorbitol before counting and imaging. Structure formation was quantitated by counting the total number of cells and the number of cells with structures from at least 250 cells and is reported as the percentage of cells with structures.

Construction of yeast strains

Generation of mCherry/mNeonGreen. Plasmids pBS34 (mCherry/KanMX6) or pBS35 (mCherry/HygromycinB) were used to generate mCherry-tagging cassettes via PCR and transformed into the appropriate GFP background strain. Plasmid pKT-mNeonGreen-His3MX6 (gift from the Zid lab, University of California [UC] San Diego) was used to generate mNeonGreen-tagging cassettes via PCR and transformed into the BY4741 background strain.

The positive clones were validated by PCR and fluorescence microscopy. In all cases, the primers were designed according to established protocols (http://depts.washington.edu/yeastrc/pages/pBS34.html), except that 10 additional nucleotides were added to the homology sequence of the gene of interest to improve the efficiency of homologous recombination.

Generation of HA-tagged strains. The 3HA-KanMX6 cassette was PCR amplified from pFA6a-3HA-kanMX6 in the same manner as the mCherry cassettes and transformed into yeast strain BY4741, using the lithium acetate/PEG method (Ito *et al.*, 1983). Positive clones were verified by PCR and indirect immunofluorescence.

Construction of Ade4p feedback inhibition–resistant yeasts. The full-length *ADE4* coding sequence was amplified from genomic DNA isolated from yeast strain BY4741 using primers that introduced an *Sal*I site at the start of the gene and an *Sma*I site at the end of the gene. The *ADE4* coding sequence was then subcloned into pFA6a-GFP-kanMX6 upstream of the GFP cassette. Site directed mutagenesis was then used to introduce the K333Q mutation into *ADE4* in the pFA6a-*ADE4*-GFP-kanMX6 plasmid (primers available on request). After the K333Q mutation was verified by sequencing, the *ade4*(K333Q)-GFP-kanMX6 cassette was PCR-amplified with primers containing 50 base pairs upstream of the *ADE4* start codon and 50 base pairs downstream of the *ADE4* stop codon. The PCR product was then transformed into yeast strain BY4741 using the lithium acetate/PEG method (Ito *et al.*, 1983). Transformants were selected on YPD agar plate containing G418 (400 μg/ml) and verified by sequencing.

Yeast strains for epitasis studies. Strains from the GFP collection (*MATa his3Δ1 leu2Δ0 met15Δ0 ura3Δ0*) were crossed with specific strains from the yeast knockout collection (*MATα his3Δ1 leu2Δ0 lys2Δ0 ura3Δ0*; gift from Maho Niwa, UC San Diego). The crosses were plated onto YPD plates and restreaked onto Met^-/Lys^- double-dropout plates to select for diploid cells. Single colonies were then inoculated into 2 ml YPD and incubated for 8 h at 30°C. The cells were washed and resuspended in 1 ml Spo-UL medium (0.1% yeast extract; 1% potassium acetate; 0.05% dextrose; 0.002% leucine; 0.004% uracil) and grown for 5–6 d on a rotator at room temperature. Tetrads were then digested with 200 U/ml zymolase (Zymo Research) and microdissected into single cells on YPD plates, followed by growth at 30°C for 48 h. Colonies were gridded onto YPD plates and grown overnight. The master plate was then replica-plated on either $G418^+$ YPD or SC-His dropout plates and grown overnight. Each haploid was genotyped by PCR or growth on selective media to ensure the presence of the GFP, the deletion, and the markers of our standard strain background (*his3Δ1 leu2Δ0 met15Δ0 ura3Δ0).*

Mitochondrial staining

For MitoTracker Red staining, GFP-tagged strains were grown to either log phase or 1 d in YPD at 30°C with shaking. MitoTracker Red (Life Technologies) was added to the culture to a final concentration of 0.1 μM and incubated at room temperature on a rotatory platform in the dark for 30 min. Cells were then washed once, resuspended in 1 M sorbitol, and imaged immediately.

For TMRE (tetramethylrhodamine, ethyl ester; Sigma Aldrich), GFP-tagged strains were grown to either log phase or 1 d in YPD at 30°C with shaking. Cells were pelleted and washed in 1X phosphate-buffered saline (PBS). Next, TMRE was added to samples to a final concentration of 5 nM and incubated at room temperature on a rotatory platform in the dark for 15 min. Cells were then washed once and resuspended in 1X PBS and imaged immediately.

Fluorescence microscopy and image analysis

Images from screening the Yeast GFP collection, MitoTracker Red, and colocalization experiments were acquired using a DeltaVision system with an Olympus IX70 microscope, an Olympus PlanApo 60×/1.40 Oil objective, and SoftWoRx software version 2.5 (Applied Precision). Images for mitochondrial staining using the pVTU-mito-dsRed plasmid and TMRE, as well as RNA granule colocalization, were taken using a Zeiss Axiovert 200M fluorescence microscope equipped with a CSU-X1 spinning disk (Yokogawa), an iChromeMLE laser source (Toptica Photonics), and μManager version 1.4 software. For each acquisition, a 2-μm Z-stack was taken with slices at 0.25-μm intervals using the 40× (or 100× for intensity ratio determination) objective.

For colocalization experiments, cells were then grown to stages where formation of the GFP-tagged structure was greatest and then fixed in 4% formaldehyde (with the exception of *IMD2::GFP*, *IMD3::GFP*, and *IMD4::GFP*) before imaging. For RNA granule and chaperone colocalization experiments, images were taken and then analyzed on ImageJ and colocalization was determined by examining each confocal slice image. Independent experiments were repeated at least three times for graphing (mean ± SEM).

Protein extraction and Western blotting

Whole cell extracts were prepared via NaOH extraction according to Kushnirov (2000). Briefly, 2.5 OD_{600} cells were harvested, resuspended in 0.1N NaOH, and incubated at room temperature for 5 min. Following centrifugation, cell pellets were resuspended in 2× sample buffer and subsequently boiled for 5 min at 95°C. Cell lysates were then resolved by 10% SDS–PAGE. Proteins were transferred to a nitrocellulose membrane (GE Amersham) by electroblotting (Owl HEP-1; Thermo Scientific). Then the standard protocol for Western blot was performed. To detect GFP-tagged proteins, 1:5000 rabbit anti-GFP (Torrey Pines Biolabs) was used as a primary antibody and 1:10,000 ECL donkey anti-rabbit immunoglobulin G (IgG), horseradish peroxidase-linked whole antibody (GE Healthcare UK) as a secondary antibody. For internal loading–control detection, 1:10,000 mouse anti–3-phosphoglycerate kinase (yeast) IgG1 monoclonal antibody (Invitrogen) was used as a primary antibody and 1:2500 ECL sheep anti-mouse IgG, horseradish peroxidase-linked whole antibody (GE Healthcare UK) as a secondary antibody.

Media shift experiments

For disassembly experiments, yeast strains were grown in YPD at 30°C with shaking for the indicated number of days and subsequently washed once and resuspended into new media (YPD, YP, 2% glucose, or water). Cells were then incubated for 30 min at 30°C with rocking and immediately imaged. Cells were also taken for protein extraction followed by Western blot analysis.

For assembly experiments, yeast strains were grown to log phase in SD media, washed once with new media (SD, SD lacking glucose, SD lacking adenine, or SD lacking glucose and adenine), and resuspended in appropriate media. Cells were incubated for 30 min at 30°C with rocking and immediately imaged. All experiments were independently repeated three times and illustrated as percentages of cells with visible structures (mean ± SEM).

Yeast indirect immunofluorescence

Indirect immunofluorescence was performed as previously described (Noree *et al.*, 2010).

Generation of anti-PRPS1 antibody

The full-length coding region of PRPS1 was cloned into pProEx-Htc and expressed as an N-terminal 6xHis-tagged fusion protein in BL21 (DE3) *E. coli*. Soluble His-PRPS1 was purified using a Ni-nitrilotriacetic acid affinity column, eluted with imidazole, and injected into rabbits (antiserum production by Covance). The antiserum was purified against 6xHis-PRPS1 protein on a CnBr-activated sepharose 4B (GE Healthcare) column.

PRPS1 immunostaining

Immunostaining and microscopy for *Drosophila* egg chambers were performed as previously described (Wilhelm *et al*., 2003). Immunostaining and microscopy for rat neurons was performed as previously described (Noree *et al*., 2010). For fibroblast staining, primary fibroblasts (R. Naviaux, UC San Diego) were plated on coverslips and cultured for 5 d at 37°C and 5% CO_2 in MEM (Invitrogen) supplemented with 10% fetal bovine serum (Cellgro), 1% L-glutamine (Invitrogen), and 1% penicillin streptomycin (Invitrogen). Fibroblasts were fixed by incubating in 4% paraformaldehyde in PBS for 20 min. The coverslips were then rinsed with 1X PBS followed by two 5-min washes in 1X PBS. The cells were incubated for 17 min at room temperature in permeabilization solution (PBS with 1% goat serum and 0.5% Triton X-100) followed by three 5-min washes in blocking solution (PBS and 1% goat serum). The coverslips were incubated overnight at 4°C in primary antibody diluted in blocking solution. The cells were washed twice for 5 min using blocking solution and then incubated for 2 h at room temperature in secondary antibody diluted in blocking solution. The secondary antibody was then aspirated to incubate for 10 min in 4′,6-diamidino-2-phenylindole (DAPI) diluted in blocking solution and rinsed quickly, followed by three 5-min washes in blocking solution. This was followed by a quick wash in water. The coverslips were mounted using Vectashield (Vector Laboratories) and imaged using a laser confocal microscope (TCS SP5; Leica). The following antibodies were used for immunostaining: α-PRPS1 (1:300; this article), α–tubulin-FITC (1:150; Sigma), and α-rabbit AlexaFluor 568 (Invitrogen) secondary antibody.

ACKNOWLEDGMENTS

We thank Douglass Forbes for comments on the manuscript, Susanne Rafelski for the gift of the pVTU-mito-dsRed plasmid, and Brian Zid for the gift of the pKT-mNeonGreen plasmid. Work at the Wilhelm lab was supported by a grant from the Hughes Collaborative Innovation Award program of the Howard Hughes Medical Institute and the James Wilhelm Memorial Fund. Kyle Begovich is a Howard Hughes Medical Institute Gilliam Fellow.

REFERENCES

Adelberg EA, Umbarger HE (1953). Isoleucine and valine metabolism in *Escherichia coli*: V. alpha-Ketoisovaleric acid accumulation. J Biol Chem 205, 475–482.

An S, Kumar R, Sheets ED, Benkovic SJ (2008). Reversible compartmentalization of de novo purine biosynthetic complexes in living cells. Science 320, 103–106.

An S, Kyoung M, Allen JJ, Shokat KM, Benkovic SJ (2010). Dynamic regulation of a metabolic multi-enzyme complex by protein kinase CK2. J Biol Chem 285, 11093–11099.

Banani SF, Lee HO, Hyman AA, Rosen MK (2017). Biomolecular condensates: organizers of cellular biochemistry. Nat Rev Mol Cell Biol 18, 285–298.

Barry RM, Bitbol AF, Lorestani A, Charles EJ, Habrian CH, Hansen JM, Li HJ, Baldwin EP, Wingreen NS, Kollman JM, *et al*. (2014). Large-scale filament formation inhibits the activity of CTP synthetase. Elife 3, e03638.

Beaty NB, Lane MD (1983a). Kinetics of activation of acetyl-CoA carboxylase by citrate: relationship to the rate of polymerization of the enzyme. J Biol Chem 258, 13043–13050.

Beaty NB, Lane MD (1983b). The polymerization of acetyl-CoA carboxylase. J Biol Chem 258, 13051–13055.

Boeynaems S, Alberti S, Fawzi NL, Mittag T, Polymenidou M, Rousseau F, Schymkowitz J, Shorter J, Wolozin B, Van Den Bosch L, *et al*. (2018). Protein phase separation: a new phase in cell biology. Trends Cell Biol 28, 420–435.

Braun EL, Fuge EK, Padilla PA, Werner-Washburne M (1996). A stationary-phase gene in *Saccharomyces cerevisiae* is a member of a novel, highly conserved gene family. J Bacteriol 178, 6865–6872.

Carcamo WC, Satoh M, Kasahara H, Terada N, Hamazaki T, Chan JY, Yao B, Tamayo S, Covini G, von Muhlen CA, *et al*. (2011). Induction of cytoplasmic rods and rings structures by inhibition of the CTP and GTP synthetic pathway in mammalian cells. PLoS One 6, e29690.

Castello A, Fischer B, Eichelbaum K, Horos R, Beckmann BM, Strein C, Davey NE, Humphreys DT, Preiss T, Steinmetz LM, *et al*. (2012). Insights into RNA biology from an atlas of mammalian mRNA-binding proteins. Cell 149, 1393–1406.

Castello A, Fischer B, Frese CK, Horos R, Alleaume AM, Foehr S, Curk T, Krijgsveld J, Hentze MW (2016). Comprehensive identification of RNA-binding domains in human cells. Mol Cell 63, 696–710.

Chang CC, Keppeke GD, Sung LY, Liu JL (2018). Inter-filament interaction between IMPDH and CTPS cytoophidia. FEBS J 285, 3753–3768.

Chen XJ, Wang X, Butow RA (2007). Yeast aconitase binds and provides metabolically coupled protection to mitochondrial DNA. Proc Natl Acad Sci USA 104, 13738–13743.

Chong YT, Koh JL, Friesen H, Duffy SK, Cox MJ, Moses A, Moffat J, Boone C, Andrews BJ (2015). Yeast proteome dynamics from single cell imaging and automated analysis. Cell 161, 1413–1424.

Crowley LC, Christensen ME, Waterhouse NJ (2016). Measuring mitochondrial transmembrane potential by TMRE staining. Cold Spring Harb Protoc 12, 1092–1096.

Ditlev JA, Case LB, Rosen MK (2018). Who's in and who's out—compositional control of biomolecular condensates. J Mol Biol 430, 4666–4684.

Eisenstein RS (2000). Iron regulatory proteins and the molecular control of mammalian iron metabolism. Annu Rev Nutr 20, 627–662.

French JB, Jones SA, Deng H, Pedley AM, Kim D, Chan CY, Hu H, Pugh RJ, Zhao H, Zhang Y, *et al*. (2016). Spatial colocalization and functional link of purinosomes with mitochondria. Science 351, 733–737.

Gerhart JC, Pardee AB (1962). The enzymology of control by feedback inhibition. J Biol Chem 237, 891–896.

Haile DJ, Rouault TA, Tang CK, Chin J, Harford JB, Klausner RD (1992). Reciprocal control of RNA-binding and aconitase activity in the regulation of the iron-responsive element binding protein: role of the iron-sulfur cluster. Proc Natl Acad Sci USA 89, 7536–7540.

Hernando Y, Carter AT, Parr A, Hove-Jensen B, Schweizer M (1999). Genetic analysis and enzyme activity suggest the existence of more than one minimal functional unit capable of synthesizing phosphoribosyl pyrophosphate in *Saccharomyces cerevisiae*. J Biol Chem 274, 12480–12487.

Hernando Y, Parr A, Schweizer M (1998). PRS5, the fifth member of the phosphoribosyl pyrophosphate synthetase gene family in *Saccharomycescerevisiae*, is essential for cell viability in the absence of either PRS1 or PRS3. J Bacteriol 180, 6404–6407.

Holmes EW, Pehlke DM, Kelley WN (1974). Human IMP dehydrogenase: kinetics and regulatory properties. Biochim Biophys Acta 364, 209–217.

Hove-Jensen B (2004). Heterooligomeric phosphoribosyl diphosphate synthase of *Saccharomyces cerevisiae*: combinatorial expression of the five PRS genes in *Escherichia coli*. J Biol Chem 279, 40345–40350.

Howson R, Huh WK, Ghaemmaghami S, Falvo JV, Bower K, Belle A, Dephoure N, Wykoff DD, Weissman JS, O'Shea EK (2005). Construction, verification and experimental use of two epitope-tagged collections of budding yeast strains. Comp Funct Genomics 6, 2–16.

Ingerson-Mahar M, Briegel A, Werner JN, Jensen GJ, Gitai Z (2010). The metabolic enzyme CTP synthase forms cytoskeletal filaments. Nat Cell Biol 12, 739–746.

Ito H, Fukuda Y, Murata K, Kimura A (1983). Transformation of intact yeast cells treated with alkali cations. J Bacteriol 153, 163–168.

Jang S, Nelson JC, Bend EG, Rodriguez-Laureano L, Tueros FG, Cartagenova L, Underwood K, Jorgensen EM, Colon-Ramos DA (2016). Glycolytic enzymes localize to synapses under energy stress to support synaptic function. Neuron 90, 278–291.

Jin M, Fuller GG, Han T, Yao Y, Alessi AF, Freeberg MA, Roach NP, Moresco JJ, Karnovsky A, Baba M, *et al*. (2017). Glycolytic enzymes coalesce in G bodies under hypoxic stress. Cell Rep 20, 895–908.

Joyner RP, Tang JH, Helenius J, Dultz E, Brune C, Holt LJ, Huet S, Muller DJ, Weis K (2016). A glucose-starvation response regulates the diffusion of macromolecules. Elife 5, e09376.
Keppeke GD, Calise SJ, Chan EK, Andrade LE (2015). Assembly of IMPDH2-based, CTPS-based, and mixed rod/ring structures is dependent on cell type and conditions of induction. J Genet Genomics 42, 287–299.
Kushnirov VV (2000). Rapid and reliable protein extraction from yeast. Yeast 16, 857–860.
Lackner LL (2019). The expanding and unexpected functions of mitochondria contact sites. Trends Cell Biol 29, 580–590.
Levitzki A, Koshland DE Jr (1972). Role of an allosteric effector: guanosine triphosphate activation in cytosine triphosphate synthetase. Biochemistry 11, 241–246.
Li S, Lu Y, Peng B, Ding J (2007). Crystal structure of human phosphoribosylpyrophosphate synthetase 1 reveals a novel allosteric site. Biochem J 401, 39–47.
Liao Y, Castello A, Fischer B, Leicht S, Foehr S, Frese CK, Ragan C, Kurscheid S, Pagler E, Yang H, *et al*. (2016). The cardiomyocyte RNA-binding proteome: links to intermediary metabolism and heart disease. Cell Rep 16, 1456–1469.
Liu JL (2010). Intracellular compartmentation of CTP synthase in *Drosophila*. J Genet Genomics 37, 281–296.
Liu JL (2016). The cytoophidium and its kind: filamentation and compartmentation of metabolic enzymes. Annu Rev Cell Dev Biol 32, 349–372.
Lynch EM, Hicks DR, Shepherd M, Endrizzi JA, Maker A, Hansen JM, Barry RM, Gitai Z, Baldwin EP, Kollman JM (2017). Human CTP synthase filament structure reveals the active enzyme conformation. Nat Struct Mol Biol 24, 507–514.
Mazumder A, Pesudo LQ, McRee S, Bathe M, Samson LD (2013). Genome-wide single-cell-level screen for protein abundance and localization changes in response to DNA damage in *S. cerevisiae*. Nucleic Acids Res 41, 9310–9324.
Meredith MJ, Lane MD (1978). Acetyl-CoA carboxylase: evidence for polymeric filament to protomer transition in the intact avian liver cell. J Biol Chem 253, 3381–3383.
Misonou Y, Kikuchi M, Sato H, Inai T, Kuroiwa T, Tanaka K, Miyakawa I (2014). Aldehyde dehydrogenase, Ald4p, is a major component of mitochondrial fluorescent inclusion bodies in the yeast *Saccharomyces cerevisiae*. Biol Open 3, 387–396.
Mitchell SF, Jain S, She M, Parker R (2013). Global analysis of yeast mRNPs. Nat Struct Mol Biol 20, 127–133.
Miyakawa I (2017). Organization and dynamics of yeast mitochondrial nucleoids. Proc Jpn Acad Ser B Phys Biol Sci 93, 339–359.
Miyakawa I, Aoi H, Sando N, Kuroiwa T (1984). Fluorescence microscopic studies of mitochondrial nucleoids during meiosis and sporulation in the yeast, *Saccharomyces cerevisiae*. J Cell Sci 66, 21–38.
Munder MC, Midtvedt D, Franzmann T, Nuske E, Otto O, Herbig M, Ulbricht E, Muller P, Taubenberger A, Maharana S, *et al*. (2016). A pH-driven transition of the cytoplasm from a fluid- to a solid-like state promotes entry into dormancy. Elife 5, e09347.
Narayanaswamy R, Levy M, Tsechansky M, Stovall GM, O'Connell JD, Mirrielees J, Ellington AD, Marcotte EM (2009). Widespread reorganization of metabolic enzymes into reversible assemblies upon nutrient starvation. Proc Natl Acad Sci USA 106, 10147–10152.
Noree C (2018). Extramitochondrial assembly of mitochondrial targeting signal disrupted mitochondrial enzyme aldehyde dehydrogenase. Sci Rep 8, 6186.
Noree C, Sato BK, Broyer RM, Wilhelm JE (2010). Identification of novel filament-forming proteins in *Saccharomyces cerevisiae* and *Drosophila melanogaster*. J Cell Biol 190, 541–551.
O'Connell JD, Tsechansky M, Royal A, Boutz DR, Ellington AD, Marcotte EM (2014). A proteomic survey of widespread protein aggregation in yeast. Mol Biosyst 10, 851–861.
O'Connell JD, Zhao A, Ellington AD, Marcotte EM (2012). Dynamic reorganization of metabolic enzymes into intracellular bodies. Annu Rev Cell Dev Biol 28, 89–111.
Pardee AB, Yates RA (1956). Control of pyrimidine biosynthesis in *Escherichia coli* by a feed-back mechanism. J Biol Chem 221, 757–770.
Petrovska I, Nuske E, Munder MC, Kulasegaran G, Malinovska L, Kroschwald S, Richter D, Fahmy K, Gibson K, Verbavatz JM, *et al*. (2014). Filament formation by metabolic enzymes is a specific adaptation to an advanced state of cellular starvation. Elife 3, e02409.
Pinson B, Vaur S, Sagot I, Coulpier F, Lemoine S, Daignan-Fornier B (2009). Metabolic intermediates selectively stimulate transcription factor interaction and modulate phosphate and purine pathways. Genes Dev 23, 1399–1407.
Protter DSW, Parker R (2016). Principles and properties of stress granules. Trends Cell Biol 26, 668–679.
Rebora K, Desmoucelles C, Borne F, Pinson B, Daignan-Fornier B (2001). Yeast AMP pathway genes respond to adenine through regulated synthesis of a metabolic intermediate. Mol Cell Biol 21, 7901–7912.
Saad S, Cereghetti G, Feng Y, Picotti P, Peter M, Dechant R (2017). Reversible protein aggregation is a protective mechanism to ensure cell cycle restart after stress. Nat Cell Biol 19, 1202–1213.
Scherrer T, Mittal N, Janga SC, Gerber AP (2010). A screen for RNA-binding proteins in yeast indicates dual functions for many enzymes. PLoS One 5, e15499.
Shah KH, Nostramo R, Zhang B, Varia SN, Klett BM, Herman PK (2014). Protein kinases are associated with multiple, distinct cytoplasmic granules in quiescent yeast cells. Genetics 198, 1495–1512.
Shen QJ, Kassim H, Huang Y, Li H, Zhang J, Li G, Wang PY, Yan J, Ye F, Liu JL (2016). Filamentation of metabolic enzymes in *Saccharomyces cerevisiae*. J Genet Genomics 43, 393–404.
Smith JL (1998). Glutamine PRPP amidotransferase: snapshots of an enzyme in action. Curr Opin Struct Biol 8, 686–694.
Srere PA (1987). Complexes of sequential metabolic enzymes. Annu Rev Biochem 56, 89–124.
Switzer RL, Sogin DC (1973). Regulation and mechanism of phosphoribosylpyrophosphate synthetase: V. Inhibition by end products and regulation by adenosine diphosphate. J Biol Chem 248, 1063–1073.
Tkach JM, Yimit A, Lee AY, Riffle M, Costanzo M, Jaschob D, Hendry JA, Ou J, Moffat J, Boone C, *et al*. (2012). Dissecting DNA damage response pathways by analysing protein localization and abundance changes during DNA replication stress. Nat Cell Biol 14, 966–976.
Van der Weyden MB, Kelly WN (1974). Human adenylosuccinate synthetase: partial purification, kinetic and regulatory properties of the enzyme from placenta. J Biol Chem 249, 7282–7289.
Webb BA, Dosey AM, Wittmann T, Kollman JM, Barber DL (2017). The glycolytic enzyme phosphofructokinase-1 assembles into filaments. J Cell Biol 216, 2305–2313.
Werner-Washburne M, Braun E, Johnston GC, Singer RA (1993). Stationary phase in the yeast *Saccharomyces cerevisiae*. Microbiol Rev 57, 383–401.
Wilhelm JE, Hilton M, Amos Q, Henzel WJ (2003). Cup is an eIF4E binding protein required for both the translational repression of oskar and the recruitment of Barentsz. J Cell Biol 163, 1197–1204.
Wyngaarden JB (1976). Regulation of purine biosynthesis and turnover. Adv Enzyme Regul 14, 25–42.
Zelenaya-Troitskaya O, Perlman PS, Butow RA (1995). An enzyme in yeast mitochondria that catalyzes a step in branched-chain amino acid biosynthesis also functions in mitochondrial DNA stability. EMBO J 14, 3268–3276.
Zhang B, Shi Q, Varia SN, Xing S, Klett BM, Cook LA, Herman PK (2016). The activity-dependent regulation of protein kinase stability by the localization to P-Bbodies. Genetics 203, 1191–1202.
Zhao A, Tsechansky M, Ellington AD, Marcotte EM (2014). Revisiting and revising the purinosome. Mol Biosyst 10, 369–374.
Zhao A, Tsechansky M, Swaminathan J, Cook L, Ellington AD, Marcotte EM (2013). Transiently transfected purine biosynthetic enzymes form stress bodies. PLoS One 8, e56203.
Zhou G, Charbonneau H, Colman RF, Zalkin H (1993). Identification of sites for feedback regulation of glutamine 5-phosphoribosylpyrophosphate amidotransferase by nucleotides and relationship to residues important for catalysis. J Biol Chem 268, 10471–10481.
Zimmer HG (1992). The oxidative pentose phosphate pathway in the heart: regulation, physiological significance, and clinical implications. Basic Res Cardiol 87, 303–316.